Simultaneous Closed-loop Control of the Current Profile and the Electron Temperature Profile in the TCV Tokamak

Justin E. Barton, William P. Wehner, Eugenio Schuster, Federico Felici and Olivier Sauter

***Abstract*— Two key properties that are often used to define a plasma operating scenario in nuclear fusion tokamak devices are the current and electron temperature (T_e) profiles due to their intimate relationship to plasma performance and stability. In the tokamak community, the current profile is typically specified in terms of the safety factor (q) profile or its inverse, the rotational transform ($\iota = 1/q$) profile. The plasma poloidal magnetic flux (Ψ) and T_e dynamics are governed by an infinite-dimensional, nonlinear, coupled, physics-based model that is described by the magnetic diffusion equation and the electron heat transport equation. In this work, an integrated feedback controller is designed to track target ι (proportional to the spatial gradient of Ψ) and T_e profiles by embedding these partial differential equation models into the control design process. The electron thermal conductivity profile is modeled as an uncertainty, and the controller is designed to be robust to an expected uncertainty range. The performance of the integrated ι + T_e profile controller in the TCV tokamak is demonstrated through simulations with the simulation code RAPTOR by first tracking a nominal target, and then modulating the T_e profile between equilibrium points while maintaining the ι profile in a stationary condition.**

I. Introduction

Nuclear fusion is the process by which two light nuclei combine together. Energy generated from these reactions can be used to produce electrical power through a conventional Rankine cycle. However, many technological challenges still need to be solved in order to develop a commercial fusion power plant. Due to the Coulombic repulsion force that exists between the positively charged nuclei, they must be heated to very high temperatures so that the nuclei possess enough kinetic energy to get close enough to fuse. At these temperatures, the fusion reactants are in the plasma state. The tokamak [1] machine employs a helical magnetic field structure to confine the plasma in a fixed toroidal volume and create the conditions necessary for fusion to occur by exploiting the plasma's ability to conduct electrical current.

In order to meet the objectives of the ITER tokamak project [2] (next phase of tokamak development), extensive research has been conducted to find plasma operating scenarios characterized by a high fusion gain and magnetohydrodynamic (MHD) stability where a dominant fraction of the current flowing in the plasma is generated by noninductive means [3]. Two key properties that are often used to define a plasma operating scenario are the current and electron temperature (T_e) profiles due to the intimate relationship these quantities have to plasma performance [4] and stability [5]. Therefore, the development of plasma profile control algorithms has the potential to improve the performance and reproducibility of tokamak operating scenarios. In the tokamak community, the current profile is typically specified in terms of the safety factor (q) profile. Advances towards developing first-principles-driven (FPD), physics-model-based algorithms for q profile control in various tokamaks are discussed in [6]–[17]. Additionally, algorithms for simultaneous control of the q profile and the volume-averaged plasma energy have been developed following both data-driven [18] and FPD [19], [20] approaches. Finally, an algorithm for q and T_e profile control based on real-time estimation of linearized static plasma profile response models is discussed in [21]. In this work, we synthesize a feedback algorithm for simultaneous q and T_e profile control in the TCV tokamak following a FPD, physics-based approach.

The plasma poloidal magnetic flux (Ψ) and electron temperature dynamics are governed by an infinite dimensional, nonlinear, coupled physics model that is described by the magnetic diffusion equation [22] and the electron heat transport equation [23]. The rotational transform (ι) profile, defined as $\iota = 1/q$, is proportional to the spatial gradient of Ψ, and therefore represents a natural plasma property conducive for feedback control. In this work, an integrated feedback controller is designed to track target ι and T_e profiles by embedding the partial differential equation (PDE) models into the design process. We model the electron thermal conductivity profile as an uncertainty and design the controller to be robust to an expected uncertainty range. The actuators used for ι and T_e profile control are the total plasma current and the auxiliary heating/current-drive (H&CD) system. The RAPTOR code [24], which is a simplified physics-based code that simulates the plasma Ψ and T_e profile dynamics, is used to test the capabilities of the controller in TCV. The integrated ι + T_e profile controller performance is demonstrated by first tracking a nominal target, and then modulating the T_e profile between equilibrium points while maintaining the ι profile in a stationary condition.

II. Plasma Profile Dynamic Models

The helical magnetic field ($\vec{B}$) in a tokamak plasma is composed of a toroidal component ($\vec{B}_\phi$) and a poloidal component ($\vec{B}_\theta$) as shown in Fig. 1. The poloidal magnetic

This material is based upon work partly supported by the U.S. Department of Energy, Office of Science, Office of Fusion Energy Sciences, under Awards DE-SC0001334 and DE-SC0010661.

J.E. Barton (justin.barton@alum.lehigh.edu), W.P. Wehner, and E. Schuster (schuster@lehigh.edu) are with the Department of Mechanical Engineering and Mechanics, Lehigh University, Bethlehem, PA 18015, USA. F. Felici is with the Control Systems Technology Group, Eindhoven University of Technology, 5600 MB Eindhoven, The Netherlands. O. Sauter is with the École Polytechnique Fédérale de Lausanne (EPFL), Centre de Recherches en Physique des Plasmas (CRPP), 1015 Lausanne, Switzerland.

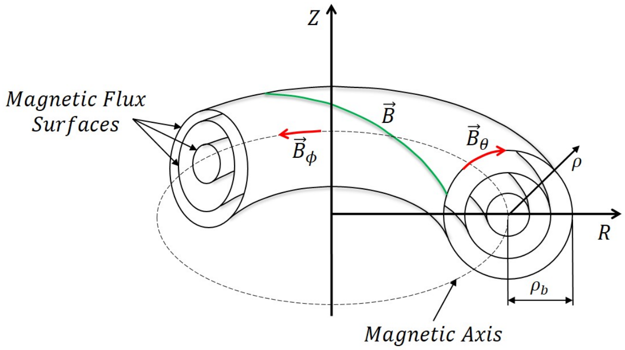

Fig. 1. Toroidal magnetic flux surfaces in a tokamak plasma. The limiting flux surface at the plasma core is called the magnetic axis and (R,Z) define the radial and vertical coordinates in the poloidal plane.

flux is defined as $\Psi = \int \vec{B}_\theta \cdot d\vec{A}_Z$, where $\vec{A}_Z$ is a disk of radius R that is perpendicular to a unit vector in the Z direction. In a well confined plasma MHD equilibrium [1], nested toroidal surfaces, which are defined by a constant poloidal magnetic flux, are obtained as shown in Fig. 1. Any quantity that is constant on these magnetic flux surfaces can be used to index them. In this work, the spatial coordinate $\hat{\rho} = \rho/\rho_b$ is used to index the magnetic flux surfaces, where ρ is a mean effective minor radius of a magnetic flux surface, i.e., $\Phi(\rho) = \pi B_{\phi,0}\rho^2$, Φ is the toroidal magnetic flux, $B_{\phi,0}$ is the vacuum toroidal magnetic field at the geometric major radius R_0 of the tokamak, and ρ_b is the mean effective minor radius of the last closed magnetic flux surface.

The rotational transform is related to the spatial gradient of the poloidal magnetic flux and is defined as

$$\iota(\hat{\rho},t) = 1/q(\hat{\rho},t) = -d\Psi/d\Phi = -[\partial\psi/\partial\hat{\rho}]/[B_{\phi,0}\rho_b^2\hat{\rho}], \quad (1)$$

where t is the time and $\psi(\hat{\rho},t)$ is the poloidal stream function, which is closely related to $\Psi(\hat{\rho},t)$, i.e., $\Psi = 2\pi\psi$. The poloidal magnetic flux dynamics in a tokamak plasma are given by the magnetic diffusion equation [22]

$$\frac{\partial\psi}{\partial t} = \frac{\eta(T_e)}{\mu_0\rho_b^2\hat{F}^2}\frac{1}{\hat{\rho}}\frac{\partial}{\partial\hat{\rho}}\left(\hat{\rho}\hat{F}\hat{G}\hat{H}\frac{\partial\psi}{\partial\hat{\rho}}\right) + R_0\hat{H}\eta(T_e)j_{ni}, \quad (2)$$

with boundary conditions $\partial\psi/\partial\hat{\rho}(0,t) = 0$ and $\partial\psi/\partial\hat{\rho}(1,t) = -k_{I_p}I_p$, where $\eta(\hat{\rho},t)$ is the plasma resistivity, $T_e(\hat{\rho},t)$ is the electron temperature, μ_0 is the vacuum magnetic permeability, $j_{ni}(\hat{\rho},t)$ is the total noninductive current density, k_{I_p} is a geometrical constant, and $I_p(t)$ is the total plasma current. The geometric spatial factors $\hat{F}(\hat{\rho})$, $\hat{G}(\hat{\rho})$, and $\hat{H}(\hat{\rho})$ are related to the magnetic configuration of a particular plasma MHD equilibrium.

Assuming diffusion is the dominant heat transport mechanism in the tokamak plasma, the electron temperature dynamics are given by the electron heat transport equation [23]

$$\frac{3}{2}\frac{\partial}{\partial t}[n_eT_e] = \frac{1}{\rho_b^2\hat{H}}\frac{1}{\hat{\rho}}\frac{\partial}{\partial\hat{\rho}}\left[\hat{\rho}\frac{\hat{G}\hat{H}^2}{\hat{F}}\left(\chi_e n_e\frac{\partial T_e}{\partial\hat{\rho}}\right)\right] + Q_e, \quad (3)$$

with boundary conditions $\partial T_e/\partial\hat{\rho}(0,t) = 0$ and $T_e(1,t) = T_{e,bdry}$, where $n_e(\hat{\rho},t)$ is the electron density, $\chi_e(\hat{\rho},t)$ is the electron thermal conductivity, $Q_e(\hat{\rho},t)$ is the total electron heating power density, and $T_{e,bdry}$ is the electron temperature at the plasma boundary, which is assumed constant.

III. Physics-based Plasma Parameter Modeling

The plasma resistivity scales inversely with the electron temperature and is modeled by a simplified Spitzer model as

$$\eta(\hat{\rho},t) = k_{sp}(\hat{\rho})Z_{eff}/[T_e(\hat{\rho},t)^{3/2}], \quad (4)$$

where k_{sp} is a spatial profile and Z_{eff} is the effective average charge of the ions, which is assumed constant in space and time. The total noninductive current density is generated by the auxiliary sources and the bootstrap current [25], i.e.,

$$j_{ni}(\hat{\rho},t) = \sum_{i=1}^{n_{aux}} j_{aux,i}(\hat{\rho},t) + j_{bs}(\hat{\rho},t), \quad (5)$$

where $j_{aux,i}$ is the current density driven by the individual auxiliary sources, j_{bs} is the current density driven by the bootstrap current, and n_{aux} is the number of auxiliary sources. The individual auxiliary current-drives are modeled as

$$j_{aux,i}(\hat{\rho},t) = j_{aux,i}^{ref}(\hat{\rho})[T_e(\hat{\rho},t)/n_e(\hat{\rho},t)]P_{aux,i}(t), \quad (6)$$

where $j_{aux,i}^{ref}$ is a normalized reference current density deposition profile for the i-th auxiliary source, T_e/n_e represents the current-drive efficiency (for electron cyclotron current-drive [26]), and $P_{aux,i}$ is the i-th auxiliary power. The bootstrap current is a self-generated current in the plasma which arises from the radial pressure gradient that is produced by the magnetic confinement [25], and is modeled as [27], [28]

$$j_{bs}(\hat{\rho},t) = \frac{k_{JkeV}R_0}{\hat{F}}\left(\frac{\partial\psi}{\partial\hat{\rho}}\right)^{-1}\left[2\mathscr{L}_{31}T_e(\hat{\rho},t)\frac{\partial n_e}{\partial\hat{\rho}}(\hat{\rho},t) + \{2\mathscr{L}_{31} + \mathscr{L}_{32} + \alpha\mathscr{L}_{34}\}n_e(\hat{\rho},t)\frac{\partial T_e}{\partial\hat{\rho}}(\hat{\rho},t)\right], \quad (7)$$

where $\mathscr{L}_{31}(\hat{\rho})$, $\mathscr{L}_{32}(\hat{\rho})$, $\mathscr{L}_{34}(\hat{\rho})$, and $\alpha(\hat{\rho})$ depend on the magnetic configuration of a particular plasma equilibrium, $k_{JkeV} = 1.602 \times 10^{-16}$ J/keV, and we have assumed equal electron and ion densities and temperatures, respectively.

The total electron heating power density is expressed as

$$Q_e(\hat{\rho},t) = \frac{1}{k_{JkeV}}\left[Q_{e,ohm}(\hat{\rho},t) + \sum_{i=1}^{n_{aux}} Q_{e,aux_i}(\hat{\rho},t) - Q_{e,rad}(\hat{\rho},t)\right] \quad (8)$$

where $Q_{e,ohm}$ is the ohmic power density, Q_{e,aux_i} are the individual auxiliary power densities, and $Q_{e,rad}$ is the radiated power density. The ohmic power density is modeled as

$$Q_{e,ohm}(\hat{\rho},t) = j_{tor}(\hat{\rho},t)^2\eta(\hat{\rho},t), \quad (9)$$

where the total toroidal current density is expressed as $j_{tor}(\hat{\rho},t) = -\frac{1}{\mu_0\rho_b^2R_0\hat{H}}\frac{1}{\hat{\rho}}\frac{\partial}{\partial\hat{\rho}}\left(\hat{\rho}\hat{G}\hat{H}\frac{\partial\psi}{\partial\hat{\rho}}\right)$ [29]. The individual auxiliary power densities are modeled as

$$Q_{e,aux_i}(\hat{\rho},t) = Q_{aux_i}^{ref}(\hat{\rho})P_{aux_i}(t), \quad (10)$$

where $Q_{aux,i}^{ref}$ is a normalized reference power density deposition profile for the i-th auxiliary source. The radiated power density (for Bremsstrahlung radiation) is modeled as [1]

$$Q_{e,rad}(\hat{\rho},t) = k_{brem}Z_{eff}n_e(\hat{\rho},t)^2\sqrt{T_e(\hat{\rho},t)}, \quad (11)$$

where $k_{brem} = 5.5 \times 10^{-37}$ Wm^3/$\sqrt{\text{keV}}$ is the Bremsstrahlung radiation coefficient.

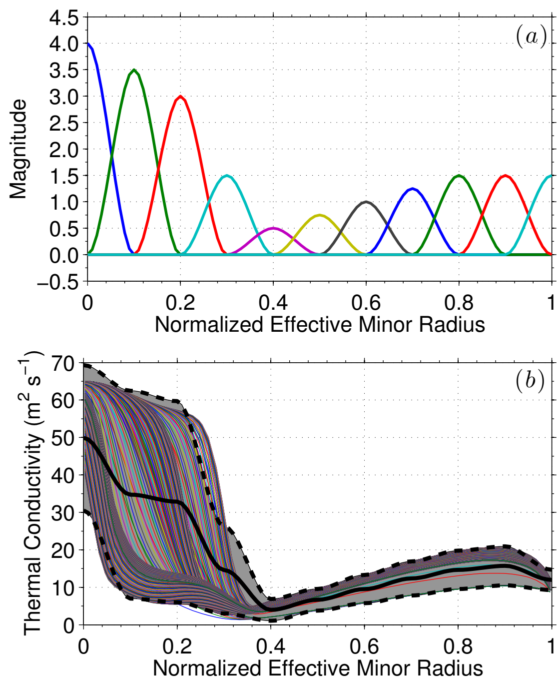

Fig. 2. (a) Cubic spline basis functions $\Lambda_\alpha(\hat{\rho})$ used to model χ_e and (b) the χ_e uncertainty range (gray-shaded region) captured by the model (12). The nominal model (characterized by $\delta_\alpha = 0$) is shown by the solid black line, and the maximum/minimum values (characterized by $\delta_\alpha = 1$ and $\delta_\alpha = -1$, respectively) are shown by the dashed black lines. The multicolored lines show the various χ_e profiles that are achieved during a typical TCV simulated discharge using RAPTOR [24]. The high central χ_e in some cases is due to MHD activity, specifically the sawtooth phenomena [1].

From (4), (6), and (7), we see that the T_e dynamics are coupled to the Ψ dynamics through resistive diffusion, auxiliary current-drive efficiency, and bootstrap current-drive. From (9), we see that the Ψ dynamics are coupled to the T_e dynamics through ohmic heating. Additionally, the local thermal transport, i.e., χ_e, is intimately dependent on the local plasma magnetic state [4]. However, it is extremely difficult to develop closed-form expressions that accurately represent this complex interaction. Therefore, in this work, we model χ_e as a nominal profile plus a bounded uncertainty. We represent χ_e by a finite number of elements n_α as

$$\chi_e(\hat{\rho}) \approx \sum_{\alpha=1}^{n_\alpha} \Lambda_\alpha(\hat{\rho})\gamma_\alpha \quad \text{where} \quad \gamma_\alpha = \gamma_\alpha^{nom} + \gamma_\alpha^{unc}\delta_\alpha, \quad (12)$$

$\Lambda_\alpha(\hat{\rho})$ are basis functions, and γ_α^{nom} and γ_α^{unc} are constants that define the range for each γ_α such that each uncertainty δ_α satisfies the condition $|\delta_\alpha| \leq 1$. The basis functions are chosen as cubic splines and are shown in Fig. 2(a). The evolution of the χ_e profile during a typical TCV simulated discharge using RAPTOR [24] is shown in Fig. 2(b). Based on this data, we can obtain values for γ_α^{nom} and γ_α^{unc} by projecting (12) onto a set of trial functions $\Lambda_\beta(\hat{\rho})$ and integrating over the spatial domain, i.e.,

$$\int_0^1 \Lambda_\beta(\hat{\rho})\chi_e(\hat{\rho})d\hat{\rho} \approx \sum_{\alpha=1}^{n_\alpha} \int_0^1 \Lambda_\beta(\hat{\rho})\Lambda_\alpha(\hat{\rho})d\hat{\rho}\,\gamma_\alpha^*. \quad (13)$$

By choosing the set Λ_β equal to the set Λ_α, (13) can be written in matrix form as $A_{\beta\alpha}\Gamma_\alpha^* = b_\beta$, where $\Gamma_\alpha^* = [\gamma_1^*, \ldots, \gamma_{n_\alpha}^*]$. For each RAPTOR simulated χ_e, we solve this matrix equation for Γ_α^*, and the parameters γ_α^{nom} and γ_α^{unc} in (12) are then calculated as $\gamma_\alpha^{nom} = [\max(\gamma_\alpha^*) + \min(\gamma_\alpha^*)]/2$ and $\gamma_\alpha^{unc} = [\max(\gamma_\alpha^*) - \min(\gamma_\alpha^*)]/2$. The χ_e uncertainty range captured by the model (12) is shown in Fig. 2(b).

IV. Feedback Control Design

The auxiliary H&CD actuators on TCV considered in this work are 4 electron cyclotron (gyrotron) launchers that are grouped into 2 clusters (denoted as a and b). The current-drive and power density deposition profiles for each source are shown in Fig. 3. The gyrotrons in cluster a are: 1 on-axis heating and co-current-injection source ($j_{ec_{1a}}^{ref}$ and $Q_{ec_{1a}}^{ref}$ in Fig. 3) and 1 off-axis heating and counter-current-injection source ($j_{ec_{2a}}^{ref}$ and $Q_{ec_{2a}}^{ref}$ in Fig. 3), and the gyrotrons in cluster b are: 1 on-axis heating and counter-current-injection source ($j_{ec_{1b}}^{ref}$ and $Q_{ec_{1b}}^{ref}$ in Fig. 3) and 1 off-axis heating and co-current-injection source ($j_{ec_{2b}}^{ref}$ and $Q_{ec_{2b}}^{ref}$ in Fig. 3). The electron density could be used for control, but in this work the electron density profile is assumed regulated around a constant profile.

By combining the magnetic diffusion equation (2) with the resistivity (4) and noninductive current-drive (5)-(7) models, and defining the quantities $f_\eta(\hat{\rho}) = k_{sp}Z_{eff}/[\mu_0\rho_b^2\hat{F}^2]$, $D_\psi(\hat{\rho}) = \hat{F}\hat{G}\hat{H}$, $g_{ec_i}(\hat{\rho}) = R_0\hat{H}k_{sp}Z_{eff}j_{ec_i}^{ref}/n_e$, $f_{bs_1}(\hat{\rho}) = k_{JkeV}R_0^2k_{sp}Z_{eff}\hat{H}/\hat{F}$, $f_{bs_2}(\hat{\rho}) = 2\mathscr{L}_{31}[dn_e/d\hat{\rho}]$, $f_{bs_3}(\hat{\rho}) = \{2\mathscr{L}_{31} + \mathscr{L}_{32} + \alpha\mathscr{L}_{34}\}n_e$, for $i \in$ [1a,2a,1b,2b], we obtain

$$\begin{aligned}\frac{\partial\psi}{\partial t} &= f_\eta \frac{1}{T_e^{3/2}}\frac{1}{\hat{\rho}}\frac{\partial}{\partial\hat{\rho}}\left(\hat{\rho}D_\psi\frac{\partial\psi}{\partial\hat{\rho}}\right)\\ &\quad + \frac{1}{T_e^{1/2}}\left(\left[g_{ec_{1a}} + g_{ec_{2a}}\right]P_{ec_a}(t) + \left[g_{ec_{1b}} + g_{ec_{2b}}\right]P_{ec_b}(t)\right)\\ &\quad + f_{bs_1}\left(\frac{\partial\psi}{\partial\hat{\rho}}\right)^{-1}\frac{1}{T_e^{3/2}}\left(f_{bs_2}T_e + f_{bs_3}\frac{\partial T_e}{\partial\hat{\rho}}\right). \end{aligned} \quad (14)$$

By combining the electron heat transport equation (3) with the electron heat source (8)-(11) and χ_e (12) models, and defining the quantities $f_{T_e}(\hat{\rho}) = [2/3][1/(\rho_b^2\hat{H}n_e)]$, $D_{T_e}(\hat{\rho}) = \hat{G}\hat{H}^2n_e/\hat{F}$, $f_{j_{tor}}(\hat{\rho}) = [2/3]k_{sp}Z_{eff}/[k_{JkeV}n_e][1/(\mu_0\rho_b^2R_0\hat{H})]^2$, $D_{j_{tor}}(\hat{\rho}) = \hat{G}\hat{H}$, $f_{rad}(\hat{\rho}) = [2/3]k_{brem}Z_{eff}n_e^2/[k_{JkeV}n_e]$, $m_{ec_i}(\hat{\rho}) = [2/3]Q_{ec_i}^{ref}/[k_{JkeV}n_e]$, for $i \in$ [1a,2a,1b,2b], we get

$$\begin{aligned}\frac{\partial T_e}{\partial t} &= f_{T_e}\frac{1}{\hat{\rho}}\frac{\partial}{\partial\hat{\rho}}\left[\hat{\rho}D_{T_e}\left(\sum_{\alpha=1}^{n_\alpha}\Lambda_\alpha\left\{\gamma_\alpha^{nom} + \gamma_\alpha^{unc}\delta_\alpha\right\}\right)\frac{\partial T_e}{\partial\hat{\rho}}\right]\\ &\quad + f_{j_{tor}}\frac{1}{\hat{\rho}^2}\left[\frac{\partial}{\partial\hat{\rho}}\left(\hat{\rho}D_{j_{tor}}\frac{\partial\psi}{\partial\hat{\rho}}\right)\right]^2\frac{1}{T_e^{3/2}} - f_{rad}T_e^{1/2}\\ &\quad + \left[m_{ec_{1a}} + m_{ec_{2a}}\right]P_{ec_a}(t) + \left[m_{ec_{1b}} + m_{ec_{2b}}\right]P_{ec_b}(t). \end{aligned} \quad (15)$$

From (1), we see that the rotational transform is related to the poloidal flux spatial gradient, which we define as $\theta(\hat{\rho},t) \equiv [\partial\psi/\partial\hat{\rho}(\hat{\rho},t)]$. Inserting this definition into (14)-(15) and after application of the chain rule, we obtain PDE models of the θ and T_e profile dynamics. Spatially discretizing these models by employing a finite difference method results in ordinary differential equation models defined by

$$\dot{\hat{\theta}} = F_\theta(\hat{\theta}, \hat{T}_e, u) \quad \dot{\hat{T}}_e = F_{T_e}(\hat{\theta}, \hat{T}_e, u, \delta) \quad \iota_i = -\frac{1}{B_{\phi,0}\rho_b^2\hat{\rho}_i}\theta_i,$$

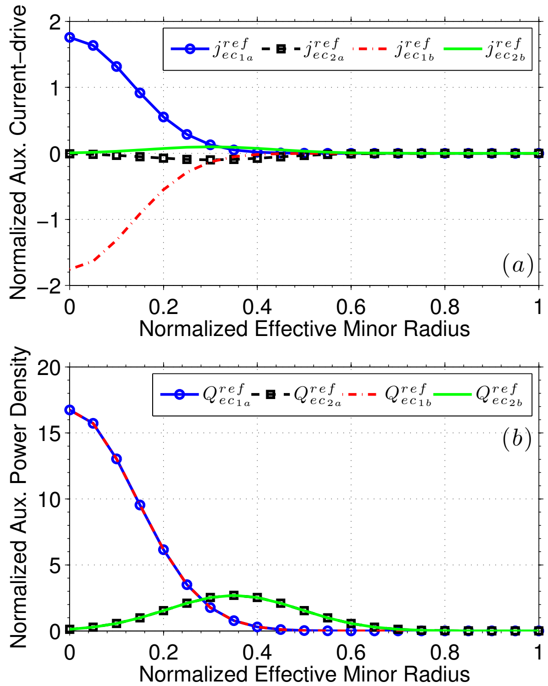

Fig. 3. Normalized auxiliary electron cyclotron (a) current-drive $\left(10^{20}\ \frac{\mathrm{m}^{-3}}{\mathrm{keV}\cdot\mathrm{W}}\cdot\frac{\mathrm{A}}{\mathrm{m}^2}\right)$ and (b) power density $\left(\mathrm{m}^{-3}\right)$ in the TCV tokamak.

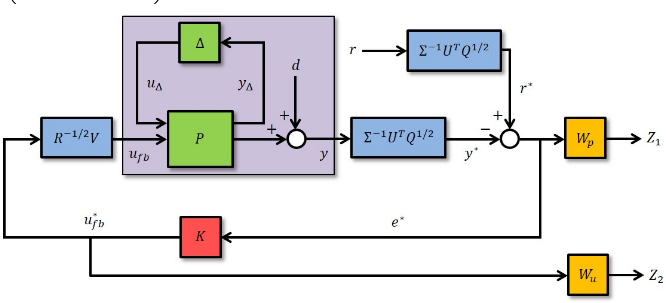

Fig. 4. Schematic of ι + T_e profile feedback control problem formulation.

where $\hat{\theta} = [\theta_2, \ldots, \theta_{m-1}] \in \mathbb{R}^n$, $\hat{T}_e = [T_{e_2}, \ldots, T_{e_{m-1}}] \in \mathbb{R}^n$, θ_i, T_{e_i}, ι_i, and $\hat{\rho}_i$ are the values of θ, T_e, ι, and $\hat{\rho}$ at the discrete nodes, for $i = [2, \ldots, m-1]$, $u = [P_{ec_a}, P_{ec_b}, I_p] \in \mathbb{R}^3$ is the control input vector, $\delta = [\delta_1, \ldots, \delta_{n_\alpha}] \in \mathbb{R}^{n\alpha}$ is the uncertain parameter vector, $F_\theta \in \mathbb{R}^n$ and $F_{T_e} \in \mathbb{R}^n$ are nonlinear functions, $n = m-2$, and m is the number of nodes used to represent the spatial domain. By defining the state vector as $x = [\hat{\theta}, \hat{T}_e] \in \mathbb{R}^{2n}$, we can write the state dynamics as

$$\dot{x} = \begin{bmatrix} F_\theta(\hat{\theta}, \hat{T}_e, u) \\ F_{T_e}(\hat{\theta}, \hat{T}_e, u, \delta) \end{bmatrix} = F_{\theta,T_e}(x, u, \delta) \in \mathbb{R}^{2n}. \qquad (16)$$

The output vector is defined as $y = [\hat{\iota}, \hat{T}_e] \in \mathbb{R}^{2n}$, where $\hat{\iota} = [\iota_2, \ldots, \iota_{m-1}] \in \mathbb{R}^n$. After linearizing (16) with respect to the state and control input around a nominal operating point $(x_{eq}, u_{eq}, 0)$, i.e., $\dot{x}_{eq} = F_{\theta,T_e}(x_{eq}, u_{eq}, 0) = 0$, we obtain

$$\dot{\tilde{x}} = A(\delta)\tilde{x} + Bu_{fb} + d_\delta \quad \text{where} \quad A(\delta) = A_0 + \sum_{i=1}^{n\alpha} \delta_i A_i, \quad (17)$$

$\tilde{x} = x - x_{eq}$, $u_{fb} = u - u_{eq}$ is the output of the to-be-designed feedback controller, $d_\delta = F_{\theta,T_e}(x_{eq}, u_{eq}, \delta)$, and $A(\delta)$ and B are the Jacobians $\partial F_{\theta,T_e}/\partial x \in \mathbb{R}^{2n\times 2n}$ and $\partial F_{\theta,T_e}/\partial u \in \mathbb{R}^{2n\times 3}$ evaluated at (x_{eq}, u_{eq}, δ). The components of the matrix $A(\delta)$ are A_0, which represents the nominal system response, and A_i, which represents the effect that the uncertain parameter δ_i has on the system response.

We now exploit the structure of the matrix $A(\delta)$ to write (17) in the conventional $P-\Delta$ robust control framework (shown in the little purple box in Fig. 4), where P is the generalized system transfer function and $\Delta = \mathrm{diag}\{\delta\}$ is a structured uncertainty matrix. The nominal model will be coupled with the uncertain parameters in the transfer function representation of (17). By employing the method outlined in [30], we can separate the uncertain parameters from the nominal parameters to write (17) in the $P-\Delta$ framework. The system input-output equations in this framework are

$$y_\Delta = P_{11}u_\Delta + P_{12}u_{fb} \qquad y = P_{21}u_\Delta + P_{22}u_{fb} + d, \quad (18)$$

where P_{11}, P_{12}, P_{21}, and P_{22} are the component transfer functions of P that describe how the system inputs (u_Δ, u_{fb}) affect the system outputs (y_Δ, y) and d represents the effect that the disturbance d_δ has on the system outputs.

The feedback system (18) is an underactuated system, i.e., there are $2n$ outputs but only 3 inputs. Therefore, at most 3 linear combinations of the system output can be controlled. In this work, we employ a singular value decomposition (SVD) of the nominal input-output relation $y = G_0(s)u_{fb}$ at a particular frequency to choose the output directions (and associated input directions) to control, where $G_0(s) = C\left(sI - A(0)\right)^{-1}B + D$ and s denotes the Laplace variable. The real approximation of the nominal input-output relation at a particular frequency $j\omega_{dc}$ is expressed as $\hat{y} = \hat{G}_0\hat{u}_{fb} = Q^{-1/2}\tilde{G}_0R^{1/2}\hat{u}_{fb} = Q^{-1/2}U\Sigma V^T R^{1/2}\hat{u}_{fb}$, where $\hat{G}_0$ denotes the real approximation of the complex matrix $G_0(j\omega_{dc})$ [31]. We define the "weighted" transfer function $\tilde{G}_0$ and its economy size SVD as $\tilde{G}_0 = Q^{1/2}\hat{G}_0R^{-1/2} = U\Sigma V^T$, where $\Sigma \in \mathbb{R}^{3\times 3}$ is a diagonal matrix of singular values, and $U \in \mathbb{R}^{2n\times 3}$ and $V \in \mathbb{R}^{3\times 3}$ are matrices that possess the following properties $V^TV = VV^T = I, U^TU = I$. We have introduced the positive definite matrices $Q \in \mathbb{R}^{2n\times 2n}$ and $R \in \mathbb{R}^{3\times 3}$ to weight the relative tracking performance and control effort.

The singular vectors of the basis for the subspace of obtainable output values ($\hat{y} = Q^{-1/2}U\Sigma\hat{y}^*$) and the corresponding input singular vectors ($\hat{u}_{fb} = R^{-1/2}V\hat{u}^*_{fb}$) are shown in Fig. 5, where $\hat{y}^*$ and $\hat{u}^*_{fb}$ are the decoupled output and input, i.e., $\hat{y}^* = \hat{u}^*_{fb}$. In this work, the frequency to evaluate the relevant channels at is chosen as $\omega_{dc} = 250$ rad/s. By examining Fig. 5, we see that this choice allows us to use the gyrotrons (P_{ec_a} and P_{ec_b} in opposite directions) to control the ι profile in the plasma core through auxiliary current-drive, the total plasma current to control the ι profile near the plasma boundary, and the gyrotrons (P_{ec_a} and P_{ec_b} in the same direction) to control the T_e profile.

The feedback control problem is formulated as shown in Fig. 4, where r is the reference value, $e = r - y$ is the tracking error ($e^* \triangleq \Sigma^{-1}U^TQ^{1/2}e \triangleq r^* - y^*$), and K is the feedback controller. The closed-loop system outputs are Z_1 and Z_2, and the frequency dependent weight functions W_p and W_u are used to optimize the feedback performance. The feedback control objectives are to maintain a small tracking error for

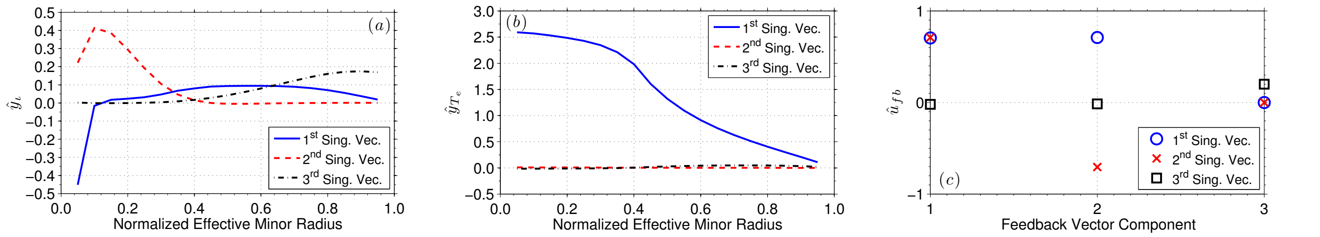

Fig. 5. Relevant control channels: (a-b) output and (c) input. The output is defined as $\hat{y} = [\hat{y}_\iota, \hat{y}_{T_e}]$, where $\hat{y}_\iota$ are the system outputs associated with the rotational transform, and $\hat{y}_{T_e}$ are the system outputs associated with the electron temperature. The feedback vector components are $u_{fb} = \left[P_{ec_a}, P_{ec_b}, I_p\right]|_{fb}$.

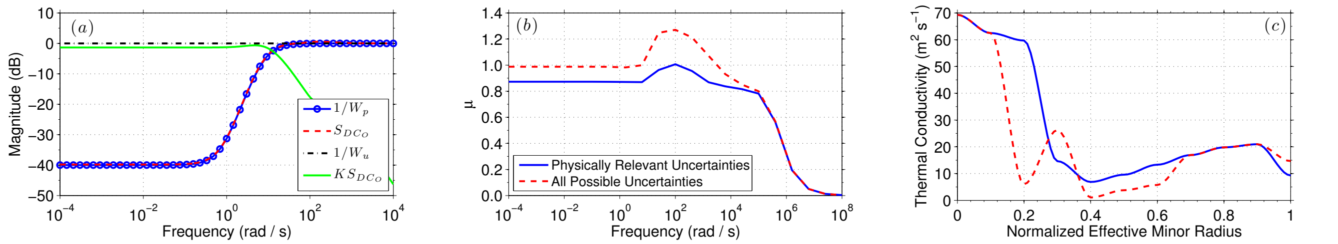

Fig. 6. (a) Nominal performance (tracking and control effort), (b) structured singular value versus frequency for physically relevant (solid) and all possible (dashed) uncertainties according to the model (12), and (c) the corresponding χ_e that results in the largest μ-value at a frequency of 100 rad/s for each respective case in (b). The robust stability condition is defined as $\mu(N_{11}(j\omega)) < 1 \ \forall\omega$ [31].

any reference, reject the effects of the external disturbance, use as little feedback control effort as possible, and robustly stabilize the system. The control problem is formulated as

$$\min_K ||T_{zw}||_\infty, \ \forall\omega \qquad T_{zw} = \begin{bmatrix} W_p S_{DC_O} & -W_p S_{DC_O} \\ W_u K S_{DC_O} & -W_u K S_{DC_O} \end{bmatrix}, \quad (19)$$

which represents the closed-loop nominal performance (NP) condition. The function T_{zw} is the closed-loop transfer function from the inputs (r^*, d^*) to the outputs (Z_1, Z_2), $d^* = \Sigma^{-1} U^T Q^{1/2} d$, and $S_{DC_O} = (I + \Sigma^{-1} U^T Q^{1/2} P_{22} R^{-1/2} V K)^{-1}$. The feedback controller is written in state-space form as

$$\dot{x}_{fb} = A^*_{fb} x_{fb} + B^*_{fb} e^* \qquad u^*_{fb} = C^*_{fb} x_{fb} + D^*_{fb} e^*, \quad (20)$$

where x_{fb} is the controller state vector, and A^*_{fb}, B^*_{fb}, C^*_{fb}, D^*_{fb} are the controller matrices obtained by solving (19).

To analyze the closed-loop system NP, the maximum singular value diagrams of the inverse of the performance weight functions and the achieved transfer functions S_{DC_O} and KS_{DC_O} are shown in Fig. 6(a). As shown, the controller achieves NP. The closed-loop system robust stability (RS) with the nominal controller is analyzed by exploiting the block-diagonal structure of Δ, which allows us to compute the structured singular value $\mu(N_{11}(j\omega))$ [31], where N_{11} is the closed-loop transfer function between the signals y_Δ and u_Δ in Fig. 4. A plot of μ versus frequency is shown in Fig. 6(b). As shown, for all possible uncertainties (dashed line in Fig. 6(b)) according to the model (12), RS is not achieved. However, by comparing the χ_e profile that results in the largest μ-value for this case (dashed line in Fig. 6(c)) to the χ_e profiles predicted by RAPTOR in Fig. 2(b), we see that the model (12) can allow unphysical χ_e profiles for the considered scenarios. Therefore, we restrict the uncertainties in the model (12) by requiring that the resulting χ_e profile safisfies $\partial\chi_e/\partial\hat{\rho} < 0$ for $\hat{\rho} \in [0, 0.35]$ and $\partial\chi_e/\partial\hat{\rho} > 0$ for $\hat{\rho} \in [0.45, 0.85]$. We then recompute μ, and as shown by the solid line in Fig. 6(b), RS is achieved for this subset of uncertainties (marginal stability is reached at 100 rad/s).

V. Control Algorithm Performance Testing

We now test the closed-loop performance of the integrated ι + T_e profile feedback controller (20) in TCV RAPTOR [24] simulations. In order to ensure a fair test of the controller performance, the target plasma state must be physically achievable, i.e., the ι and T_e profiles that are specified as targets in the simulations must be compatible with each other. In this work, we obtain T_e profiles that are compatible with specific ι profiles by executing RAPTOR simulations with ι profile control only [16] and taking the resulting T_e profile as a nominal compatible target. In this work, a q profile achieved in TCV with I_p = 190 kA and counter-current-injection auxiliary power is chosen as the target, and the corresponding nominal T_e profile has a broad profile shape.

During the simulations, the ι profile target is held constant, and the nominal T_e profile is set as the target for $t \in [0, 1)$ s. For $t \in [1, 1.4)$ s, the nominal T_e profile is scaled down by 10%, and the resulting profile is set as the target. Finally, the nominal T_e profile is scaled up by 10%, and the resulting profile is set as the target for $t \in [1.4, 2]$ s. First, a ι and T_e profile evolution is obtained by executing a feedforward-only simulation with a particular set of input trajectories. Next, the ability of the controller to track the target is determined by executing a feedforward + feedback simulation with the same feedforward input trajectories used in the first simulation.

Time traces of q and T_e at various spatial locations, and a comparison of the control inputs is shown in Fig. 7. Once the controller becomes active at 0.1 s, it is able to drive the ι and T_e profiles to the target during the nominal phase of the simulation ($t \in [0, 1)$ s) by increasing the total plasma current and the cluster b gyrotron power and decreasing the cluster a gyrotron power. During the time interval $t \in [1, 2]$ s, the controller is able to modulate the T_e profile between equilibrium points while maintaining the q profile in a relatively stationary condition by rejecting the effects that the changing T_e have on the magnetic profile dynamics.

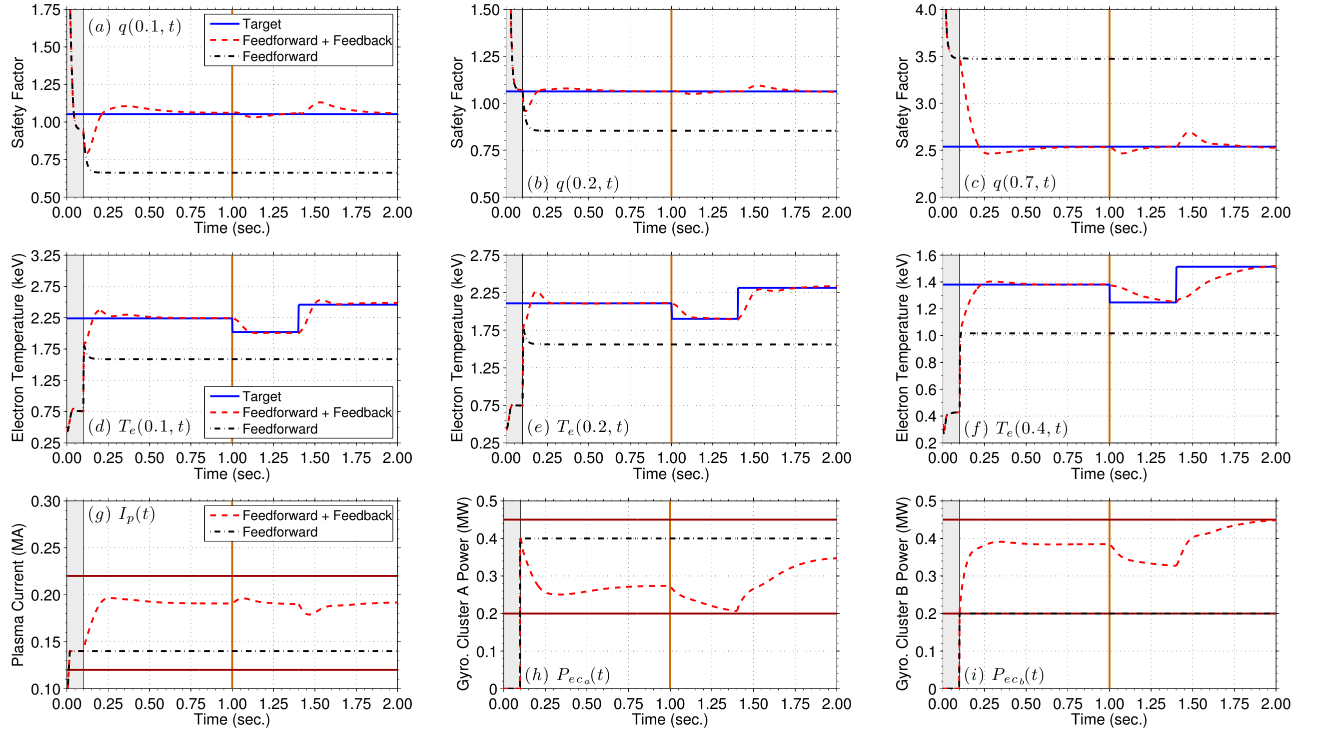

Fig. 7. Time traces of outputs (q,T_e) and inputs (I_p,P_{ec_a},P_{ec_b}). The solid-orange vertical line denotes when the target q profile is maintained in a stationary condition while modifying the T_e profile between equilibrium points. Feedback controller off (gray-shaded region) and actuator limits (solid-brown line).

VI. Conclusions and Future Work

An integrated feedback algorithm for ι and T_e profile control in tokamaks was developed following a FPD, physics-based modeling approach. The controller was designed to be robust to an expected range of uncertainty in the χ_e profile. The performance of the controller was demonstrated through RAPTOR simulations of the TCV tokamak plasma dynamics. One direction of future work is to develop a model of the χ_e that naturally predicts physically relevant profiles. Additionally, our future work includes using the closed-loop plasma state observer developed in [32] to reconstruct the ι and T_e profiles in real-time to experimentally test the controller in TCV.

References

[1] WESSON, J., *Tokamaks*, Oxford, UK: Clarendon Press, 2004.
[2] ITER Organization, [Online]. Available: http://www.iter.org.
[3] TAYLOR, T. et al., Plasma Phys. and Control. Fusion **39** (1997) B47.
[4] PETTY, C. et al., Phys. of Plasmas **5** (1998) 1695.
[5] FERRON, J. et al., Physics of Plasmas **12** (2005) 056126.
[6] OU, Y., XU, C., and SCHUSTER, E., IEEE Trans. Control Syst. Technol. **19** (2011) 432.
[7] XU, C., OU, Y., and SCHUSTER, E., Automatica **47** (2011) 418.
[8] GAYE, O. et al., Sliding Mode Stabilization of the Current Profile in Tokamak Plasmas, in *50th IEEE Conference on Decision and Control*, pp. 2638–2643, 2011.
[9] BARTON, J. E., BOYER, M. D., SHI, W., SCHUSTER, E., et al., Nucl. Fusion **52** (2012) 123018.
[10] GAHLAWAT, A. et al., Bootstrap Current Optimization in Tokamaks using Sum-of-Squares Polynomials, in *51st IEEE Conference on Decision and Control*, pp. 4359–4365, 2012.
[11] BOYER, M. D., BARTON, J. E., SCHUSTER, E., et al., Plasma Phys. Control. Fusion **55** (2013) 105007.
[12] ARGOMEDO, F. B. et al., Nuclear Fusion **53** (2013) 033005.
[13] VU, N. M. T. et al., An IDA-PBC Approach for the Control of 1D Plasma Profile in Tokamaks, in *52nd IEEE Conference on Decision and Control*, pp. 4176–81, 2013.
[14] BOYER, M. D., BARTON, J. E., SCHUSTER, E., et al., IEEE Trans. Control Syst. Technol. **22** (2014) 1725.
[15] BOYER, M. D., BARTON, J. E., SHI, W., WEHNER, W. P., SCHUSTER, E., et al., Simultaneous Boundary and Distributed Feedback Control of the Current Profile in H-mode Discharges on DIII-D, in *19th IFAC World Congress*, pp. 1568–1573, 2014.
[16] BARTON, J. E., SCHUSTER, E., FELICI, F., and SAUTER, O., Closed-loop Control of the Safety Factor Profile in the TCV Tokamak, in *53rd IEEE Conference on Decision and Control*, pp. 5660–5665, 2014.
[17] MALJAARS, E. et al., Nuclear Fusion **55** (2015) 023001.
[18] MOREAU, D. et al., Integrated Magnetic and Kinetic Control of Advanced Tokamak Scenarios based on Data-driven Models, in *24th IAEA Fusion Energy Conference*, paper ITR/P1-20, 2012.
[19] BARTON, J. E., BESSEGHIR, K., LISTER, J., and SCHUSTER, E., Robust Control of the Safety Factor Profile and Stored Energy Evolutions in High Performance Burning Plasma Scenarios in the ITER Tokamak, in *52nd IEEE Conference on Decision and Control*, pp. 4194–99, 2013.
[20] BARTON, J. E., BOYER, M. D., SHI, W., WEHNER, W. P., SCHUSTER, E., et al., Experimental and Simulation Testing of Physics-model-based Safety Factor Profile and Internal Energy Feedback Controllers in DIII-D Advanced Tokamak Scenarios, in *19th IFAC World Congress*, pp. 5223–5228, 2014.
[21] KIM, S. H. and LISTER, J. B., Nuclear Fusion **52** (2012) 074002.
[22] HINTON, F. and HAZELTINE, R., Rev. Mod. Phys. **48** (1976) 239.
[23] BASIUK, V. et al., Nucl. Fusion **43** (2003) 822.
[24] FELICI, F. et al., Nuclear Fusion **51** (2011) 083052.
[25] PEETERS, A. G., Plasma Phys. and Control. Fusion **42** (2000) B231.
[26] LUCE, T. C. et al., Physical Review Letters **83** (1999) 4550.
[27] SAUTER, O. et al., Physics of Plasmas **6** (1999) 2834.
[28] SAUTER, O. et al., Physics of Plasmas **9** (2002) 5140.
[29] PEREVERZEV, G. V. et al., ASTRA Automated System for Transport Analysis in a Tokamak, in *Technical Report 5/98 IPP Report*, 2002.
[30] PACKARD, A., *Whats New with μ: Structured Uncertainty in Multivariable Control*, PhD thesis, Univ. of Calif., Berkeley, 1988.
[31] SKOGESTAD, S. and POSTLETHWAITE, I., *Multivariable Feedback Control Analysis and Design*, Wiley, New York, 2005.
[32] FELICI, F. et al., A Dynamic State Observer for Real-time Reconstruction of the Tokamak Plasma Profile State and Disturbances, in *2014 American Control Conference*, pp. 4816–4823, 2014.